SUPPLEMENTAL INFORMATION

Spectroscopic investigation of the electrochemical growth and stability of am-hydr-IrO_x grown from IrTi alloys.

Benjamin Howchen[a,*], Marianne van der Merwe[a], Alexander Steigert[b], Raul Garcia-Diez[a], Catalina E. Jimenez[a,c], Rosario Suarez Anzorena[a,d], Roberto Félix[a,c], Ilaria Lucentini[e,f], Carlos Escudero[e], Johannes Frisch[a,c], Regan G. Wilks[a,c] and Marcus Bär [a,c,g,h,*]

[a.] *Interface Design, Helmholtz-Zentrum Berlin für Materialien und Energie GmbH (HZB), Albert-Einstein-Str. 15, 12489 Berlin,*

[b.] *· PVComB, HZB, Schwarzschildstr. 3, 12489 Berlin, Germany*

[c.] *Energy Materials In-Situ Laboratory Berlin (EMIL), HZB, Albert-Einstein-Str. 15, 12489 Berlin, Germany*

[d.] *Unidad de Investigación y Desarrollo Estratégico para la Defensa (UNIDEF-CONICET-MINDEF), CITEDEF, J.B. de La Salle 4397, B1603ALO Villa Martelli, Buenos Aires, Argentina*

[e.] *ALBA Synchrotron Light Source, Carrer de la Llum 2-26, 08290 Cerdanyola del Vallès, Barcelona, Spain*

[f.] *Department of Chemical Engineering, Universitat Politècnica de Catalunya, EEBE, Eduard Maristany 10-14, 08019 Barcelona, Spain*

[g.] *Department of Chemistry and Pharmacy, Friedrich-Alexander-Universität Erlangen-Nürnberg (FAU), Egerlandstr. 3, 91058 Erlangen, Germany*

[h.] *Helmholtz-Institute Erlangen-Nürnberg for Renewable Energy (HI ERN), Albert-Einstein-Str. 15, 12489 Berlin, Germany*

[*] *Corresponding authors.*

The raw data utilised in this work have been deposited online in a Zenodo repository that has the following permanent DOI: 10.5281/zenodo.18164742

Methods

Sample preparation. Ir_xTi_{1-x} alloys were prepared using a PREVAC sputter deposition system located in the Energy Materials In-Situ Laboratory Berlin (EMIL) facility at HZB, i.e. the sputter system is connected to the lab-based XPS (X-ray photoelectron spectroscopy) system (see below) via an interconnected Ultra-High Vacuum (UHV) system. The ~30 nm films were prepared by direct current (DC) magnetron co-sputtering of iridium, fixed at 50 W, and titanium, using 0-80 W onto a silicon substrate. The target film thickness was achieved by means of a quartz crystal microbalance and confirmed using X-ray reflectometry (XRR, see below)). Samples for Ir L_3-edge X-ray absorption spectroscopy (XAS) measurements (see below) were prepared using a similar method but using glassy carbon window (10 x 10 x 0.3 mm^3) substrates instead.

Electrochemical growth of am-hydr-IrOx. Electrochemical measurements were performed using an electrolyte of 0.5 M H_2SO_4, a 4 mm diameter glassy carbon rod (Thermo Fischer Scientific) as the counter electrode and a Mini HydroFlex reversible hydrogen electrode (Gaskatel) as the reference electrode (all potentials reported are relative to a reversible hydrogen electrode, RHE) with a Biologic SP-300 potentiostat. Am-hydr-IrOx synthesis involved potential cycling of the metallic Ir_xTi_{1-x} films prepared between 0.05 to 1.5 V vs RHE at 500 mV s^{-1}. During the initial growth and up to 1000 cycles, after every 200 cycles at 500 mV s^{-1}, a scan at 10 mV s^{-1} was performed to allow for detailed analysis. All cyclic voltammetry results are averaged from 3 independently prepared samples to ensure representative results. Samples for hard X-ray photoelectron spectroscopy (HAXPES) analysis were prepared using the same procedure, followed by drying at 60 °C for 5 hours to remove water.

Electrochemical impedance spectroscopy Electrochemical measurements were performed using an electrolyte of 0.5 M H_2SO_4, a 4 mm diameter glassy carbon rod (Thermo Fischer Scientific) as the counter electrode and a Mini HydroFlex reversible hydrogen electrode (Gaskatel) as the reference electrode (all potentials reported are relative to a reversible hydrogen electrode, RHE) with a Biologic SP-300 potentiostat. The electrochemical impedance spectra were measured at open circuit potential between 0.1 and $2x10^{-5}$ Hz with an amplitude of 10 mV. The series resistance was approximated as the high frequency response of the impedance.

X-ray photoelectron spectroscopy of pristine and post-mortem samples. Lab-based XPS measurements were conducted using a monochromatized Al K_α (1486.71 eV) SPECS FOCUS 500 source. The photoelectrons ejected were detected using a SPECS PHOIBOS 150 MCD-9 analyzer. Measurements were performed with a base pressure $<1x10^{-8}$ mbar. The pass energy for all core level spectra measurements was 20 eV, whereas 100 eV was used for the survey spectra. The binding energies of the XPS data were calibrated setting the Au $4f_{7/2}$ of a clean Au reference to 84.00 eV. Samples for post-mortem analysis were washed with deionized water, followed by drying at 60 °C for 5 hours to remove water before being measured.

The elemental surface ratios were calculated using the Ir 4f and Ti 2p XPS data for the pristine alloy films. After subtracting a linear background, the total peak area was derived by integration considering both, the oxidized and metallic, contributions for Ti. The areas were then normalized using the relative sensitivity factors. The data integration procedure is exemplarily shown for the $Ir_{74}Ti_{26}$ sample in Fig. S4 and the results are summarized in Table S1. Note that Ir 4f overlaps with the spectra of the Ti 3s and Ir $5p_{1/2}$ core level lines,[1] but their spectral contributions are considered to be negligible when probed with Al K_α; as in this case their photoionization cross sections are more than one order of magnitude smaller than that of Ir 4f.[2]

Fitting procedure for Ti 2p was performed using previously reported methods[3] with the CasaXPS software package (*Casa Software Ltd.*, UK) taking into account that due to Coster-Kronig effects, the Ti $2p_{3/2}$ and $2p_{1/2}$ core levels displays different FWHMs. Spin-orbit coupling components were constrained with a ratio of 1:2 for the $2p_{1/2}$: $2p_{3/2}$ lines. Oxide components were fit using a symmetrical peak shape profile GL(30), while for metallic components an asymmetrical peak shape LA(2,4,1) was used instead. Spin-orbit coupling components were constrained with splitting values reported in the same work.[3] Binding energy values of titanium and its oxides were obtained from van der Merwe *et al*.[1]

Hard X-ray photoelectron spectroscopy measurements. HAXPES experiments were conducted at the HiKE endstation located at BESSY II's KMC-1 bending magnet beamline at HZB.[4,5] The base pressure was $<1x10^{-8}$ mbar. The emitted photoelectrons were detected with a Scienta R4000 electron energy analyzer. The spectra were recorded using calibrated photon energies of 2.003 keV and 5.950 keV (referred to as 2 and 6 keV respectively for simplicity) using the Si(111) crystal pair of the double-crystal monochromator for energy selection. A pass energy of 200 eV was used for all measurements. Slight deviations from the photon energies were corrected by referencing the Au $4f_{7/2}$ peak of a grounded clean Au foil to a binding energy of 84.00 eV. Peaks are fit using GL(83) line shape profiles and a linear background using the CasaXPS software.

Grazing incidence X-ray diffraction (GI-XRD). All GI-XRD measurements were performed using a BRUKER D8 instrument in grazing incidence mode at an angle of 1° with a Cu K_α X-ray source having an energy of 8.04 keV.

X-ray reflectometry. The coating thickness was determined by X-ray reflectometry (XRR). The XRR measurements were carried out using an X'pro device from PANALYTICAL with a Cu K_α source (1.544 Angstrom average wavelength from alpha 1 & 2) and analysed with the software PANALYTICAL x'pert reflectivity.

Ir L_3-edge X-ray absorption spectroscopy measurements. Figure S1a depicts the used custom designed electrochemical cell, which was coupled to a Biologic SP-300 potentiostat for the *operando* measurements. **Figure S1(b)** shows the experimental configuration of the total fluorescence yield X-ray absorption spectroscopy measurements at the Ir L_3-edge performed at the DIF-XAS endstation at the NOTOS beamline of the ALBA Synchrotron[6,7] during the *in-situ* growth and potential dependent measurements of am-hydr-IrOx. The synchrotron light coming from a 1.42 T bending magnet was first vertically collimated, then monochromatized using two pairs of water-cooled Si(111) crystals and finally focused to the sample position on an area of ≈500 × 500 µm^2. The Ir L_3-edge XAS measurements were performed in fluorescence yield using a 13-element energy-resolving silicon-drift fluorescence detector (Canberra) at 45° angle with respect to the incoming X-rays (**Figure S1b**). Three DC current-type ionization chambers (Oken) were used for measuring the incoming beam intensity and the IrO_2 reference in transmission mode (**Figure S1b**). The custom-made flow cell was mounted on a motorized xyz sample stage and connected to a Biologic SP-300 potentiostat. The Ir_xTi_{1-x} samples mounted in the custom-made flow cell exposed ≈28 mm^2 of the sample area to the 0.5 M H_2SO_4 electrolyte.

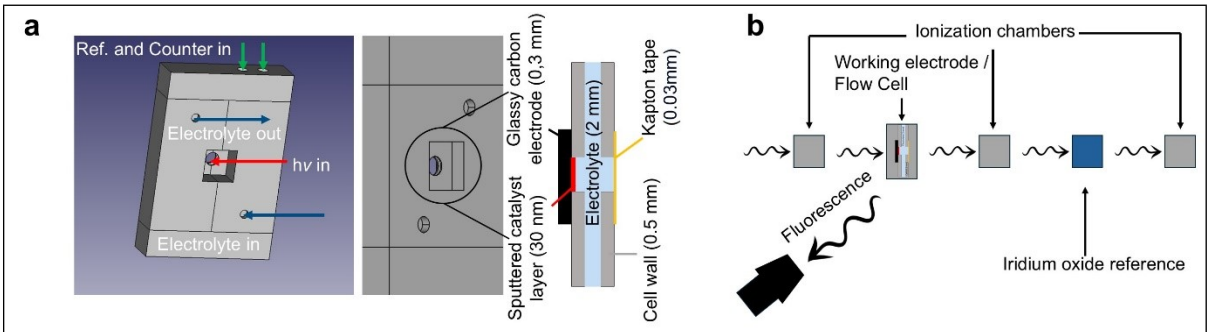

Figure S1 Custom designed electrochemical cell for *operando* XAS measurements at the NOTOS beamline located at ALBA and schematic of measurement geometry. (a) Illustration of custom-made electrochemical cell with labels detailing how electrolyte is flown through the cell, where all electrodes are placed, and the relative thicknesses of the different layers that the X-ray beam penetrates. (b) Schematic of the measurement geometry, where the sample is perpendicular to the incident X-ray beam and the fluorescence detector is located at 45° from the incident beam.

Ti K-edge X-ray absorption spectroscopy. Ti K-edge XAS measurements were performed at the HiKE Endstation located at the BESSY II KMC-1 beamline operated by HZB in reflection geometry and fluorescence yield mode,[8] using the Si (311) crystal pair of the double crystal monochromator (energy resolution of 0.5 eV at 5000 eV) and a Bruker XFlash 4010 fluorescence SDD at 10°. The base pressure was $<1 \times 10^{-8}$ mbar and the beam focus size was 0.1 mm × 0.1 mm.[9] The photon energy scale was calibrated according to the endstation standard procedure, measuring the Au $4f_{7/2}$ core level of a clean gold foil by HAXPES at excitation energies of 4920 and 5060 eV before and after each XAS scan, respectively, using a reference Au $4f_{7/2}$ binding energy of 84.00 eV. No drifts or shifts were observed through the measurements. The titanium reference samples (Ti, TiO, Ti_2O_3, Ti_4O_7, and TiO_2) were all purchased from Sigma-Aldrich.

XPS characterisation of the as prepared films

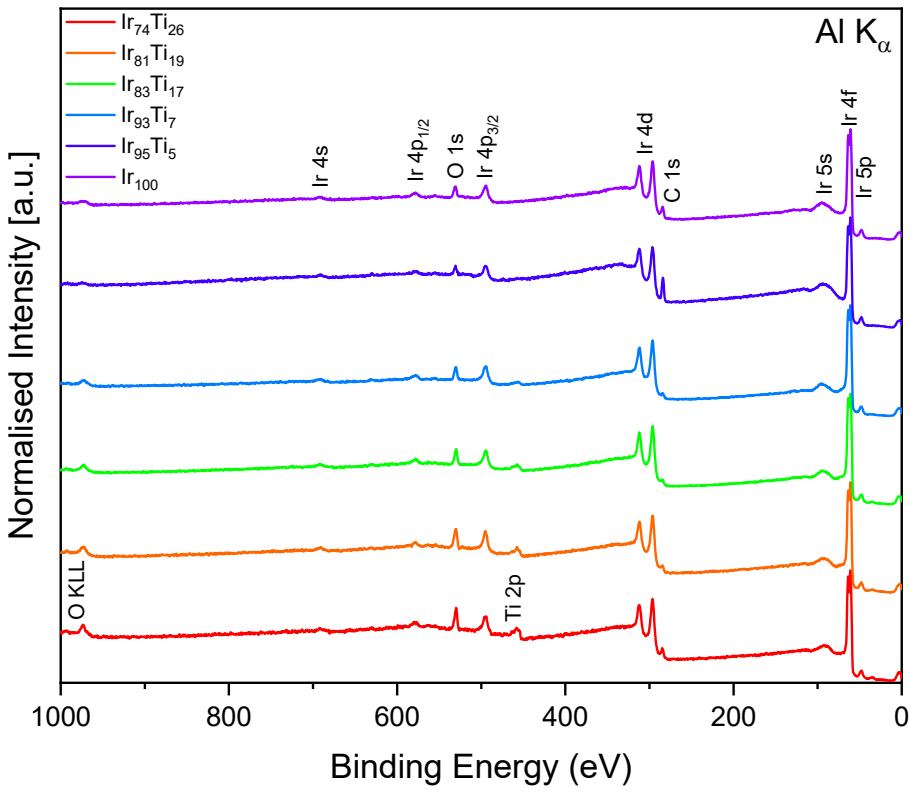

Figure S2. Al K_α excited X-ray photoelectron spectroscopy survey spectra of the pristine Ir_xTi_{1-x} samples. The spectra have been 0-to-1 normalized and a constant vertical offset was added for clarity.

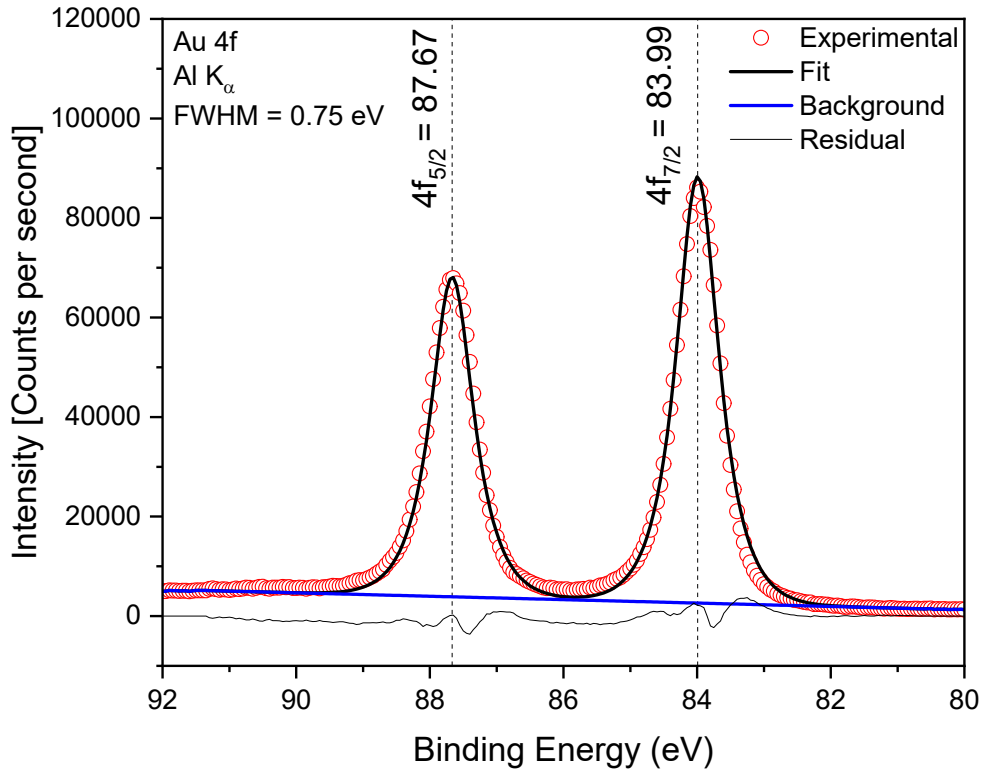

Figure S3 Al K_α excited XPS detail spectrum of Au 4f, used for calibration. Peaks are fit using GL(83) line shape and a linear background using the CasaXPS software. Spectrum was recorded using a pass energy of 20 eV. All data were calibrated by shifting the Au $4f_{7/2}$ to 84.00 eV.

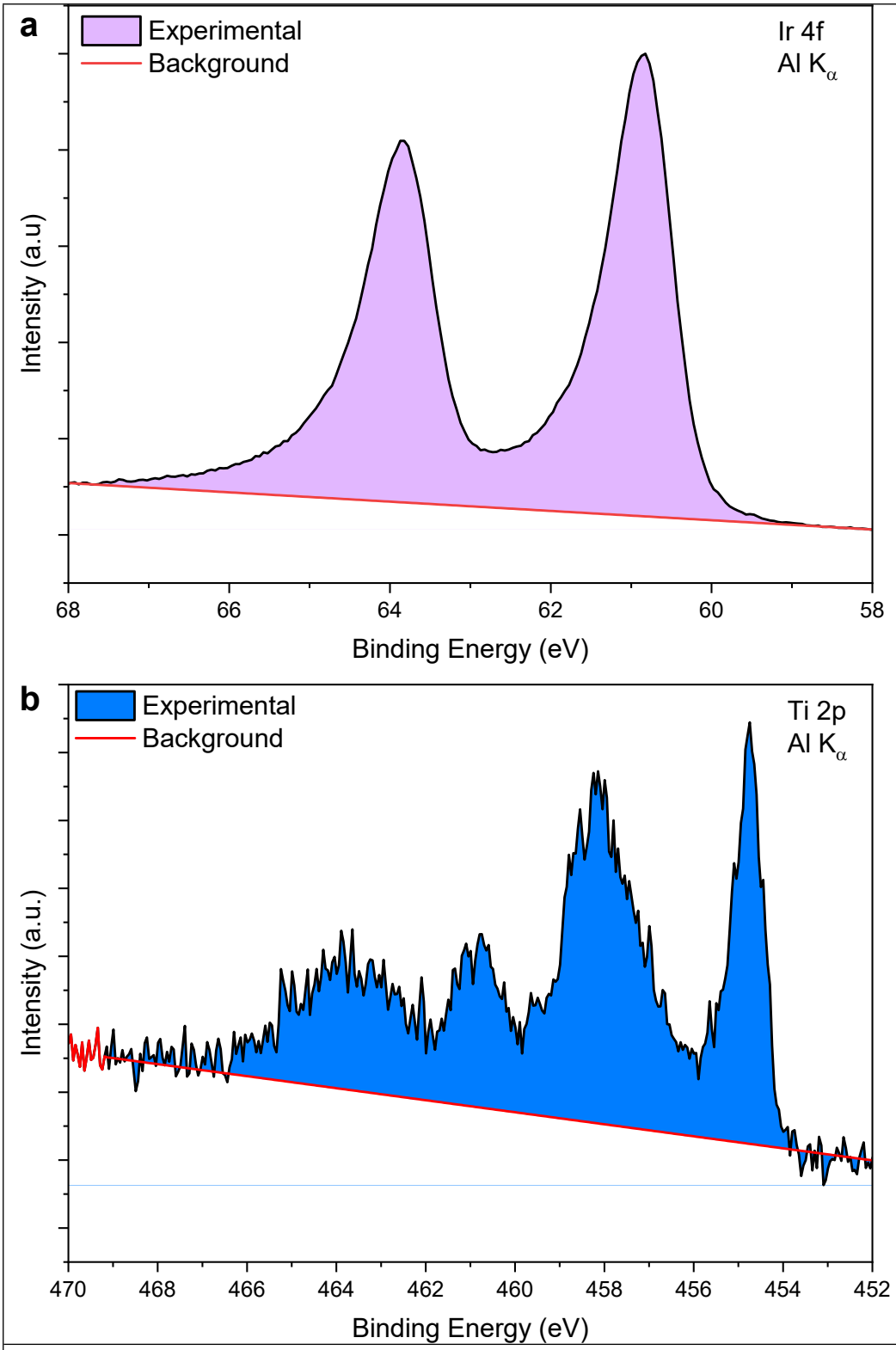

Figure S4 Quantification of Ir:Ti metal ratio. Example of peak area intensity quantification using the integrated area from the Ir 4f and Ti 2p XPS data of the $Ir_{74}Ti_{26}$ sample. Integration boundaries were kept constant, and a linear background was used.

Ti power	Ir 4f Integrated area	Ti 2p Integrated area	Ir 4f / rel. sensitivity factor (Ir 4f = 13.9)[10]	Ti 2p / rel. sensitivity factor (Ti 4f = 7.81)[10]	x = Ir/[Ir + Ti]
80	6207.7	1227.9	446.6	157.2	0.74
60	11780.4	1527.4	847.5	195.6	0.81
40	21810.4	2595.1	1569.1	332.3	0.83
20	24417.9	970.7	1756.7	124.3	0.93
10	16151.6	548.8	1162.0	70.3	0.94
0	/	/	/	/	1

Table S1 Summary of the obtained relative surface composition of the pristine Ir_xTi_{1-x} alloys

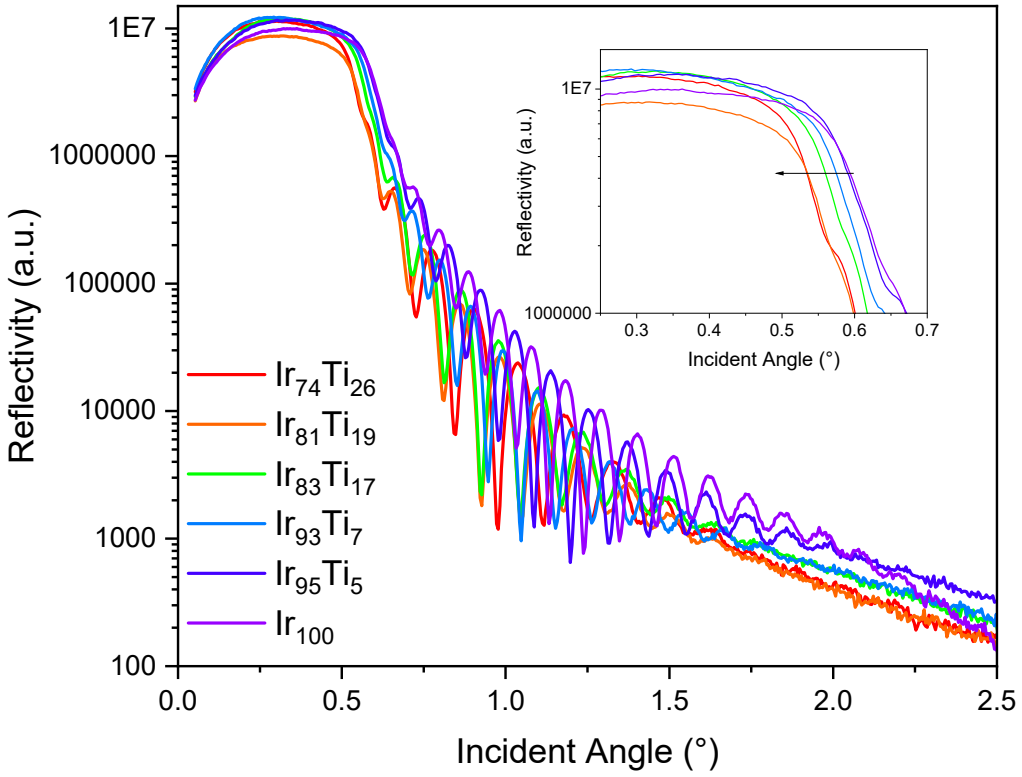

Figure S5. Analysis of film thickness. X-ray reflectometry (XRR) data. The inset shows an enlarged region of the shift of critical incident angle between samples. The critical incident angle was determined by calculating the intercept of linear extrapolations before and after the steep drop in reflectivity.

Sample	Ir power (W)	Ti power (W)	Film Thickness (nm)
$Ir_{74}Ti_{26}$	50	80	34.7
$Ir_{81}Ti_{19}$	50	60	36.7
$Ir_{83}Ti_{17}$	50	40	31.1
$Ir_{93}Ti_{7}$	50	20	30.8
$Ir_{95}Ti_{5}$	50	10	28.4
Ir_{100}	50	0	37.2

Table S2. Summary of sample film thicknesses values derived from XRR.

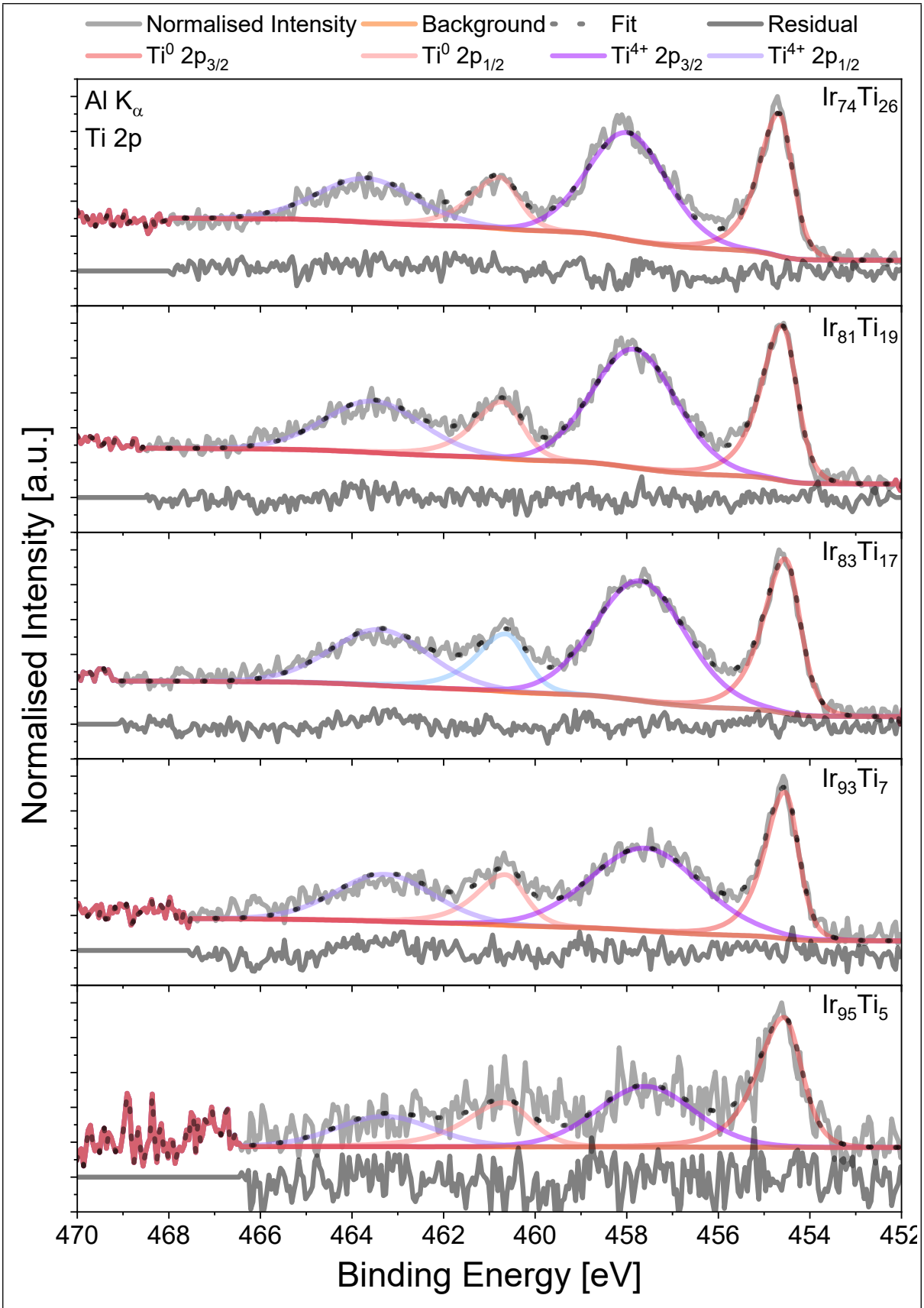

Figure S6. Fits of the Ti 2p XPS spectra of the pristine alloy films

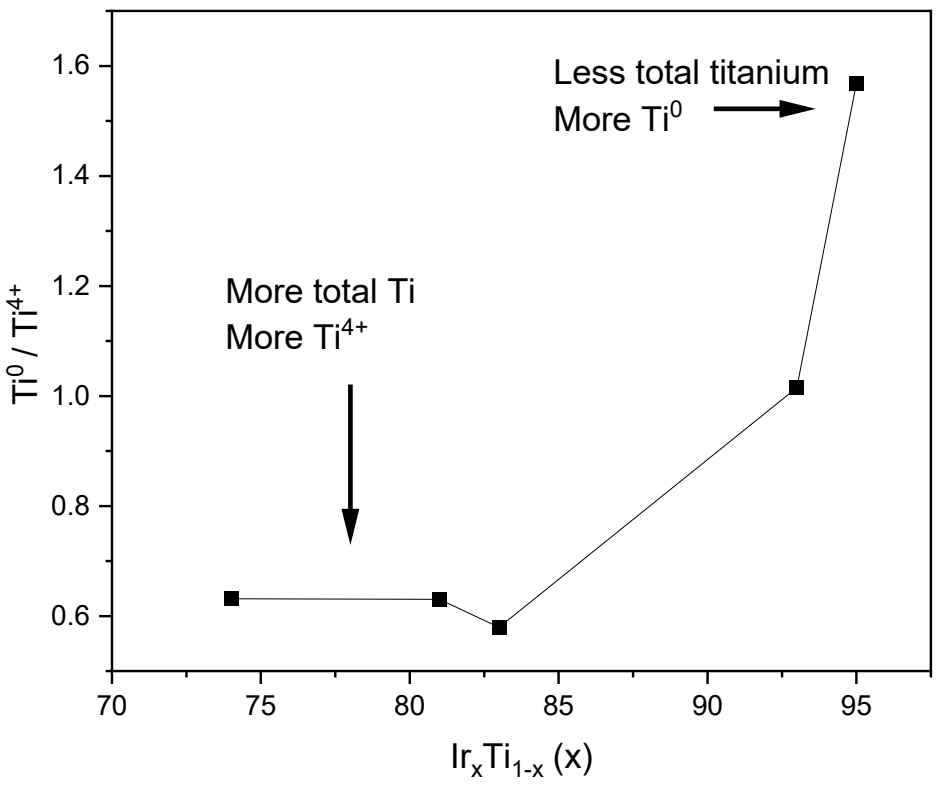

Figure S7. Metallic titanium (Ti^0) – to – oxidized titanium (Ti^{4+}) - ratio of the pristine alloy films as determined through XPS as a function of elemental surface ratio

	Integrated Areas				
Samples	**Ti^0 $2p_{1/2}$**	**Ti^0 $2p_{3/2}$**	**Ti^{4+} $2p_{1/2}$**	**Ti^{4+} $2p_{3/2}$**	**Ti^0 / Ti^{4+}**
$Ir_{74}Ti_{26}$	820.61	913.77	874.78	1022.80	0.63
$Ir_{81}Ti_{19}$	1326.28	1452.57	1400.44	1600.47	0.63
$Ir_{83}Ti_{17}$	2044.93	2208.30	2163.74	2445.37	0.58
$Ir_{93}Ti_{7}$	2091.45	2202.64	2090.68	2199.20	1.01
$Ir_{95}Ti_{5}$	2064.41	2113.16	2046.75	2077.84	0.30

Table S3 Summary of the obtained relative Ti^0/Ti^{4+} composition of the pristine Ir_xTi_{1-x} alloys

Cyclic voltammetry: growth of am-hydr-IrOx during up to 1000 cycles

The growth of the highly porous am-hydr-IrOx was performed by continuous cycling from a metallic mixed Ir_xTi_{1-x} substrate at 500 mV s^{-1} between 0.05 to 1.5 V *vs* RHE in an electrolyte composed of 0.5 M H_2SO_4. The cycling between oxidizing and partially reducing conditions leads to the layer-by-layer increase of a hydrous metal oxide layer extending from the metallic substrate. As the am-hydr-IrO_x grows, it exposes the underlying bare metal to more electrolyte, allowing for a continuous growth. This is noted through the electrochemical signature in two ways: (i) the increased capacitance, indicative of a higher surface area; as well as (ii) the increasing redox peaks, associated with more electrochemically active iridium species.

The growth of the am-hydr-IrO_x layers was tracked by measuring the integral of the redox peaks as a function of cycle number. Specifically, the area of the reductive portion of the redox couple appearing around 1.05 V vs RHE was selected and the integration range of 0.6 to 1.2 V vs RHE with a linear background was used for all samples (see Fig. S8). This area was selected to allow for an internally consistent measure of the flowing charge between all samples to avoid the influence of the small anodic redox peak appearing between 0.6 to 0.7 V vs RHE. The area is converted to absolute charge using the equation below.

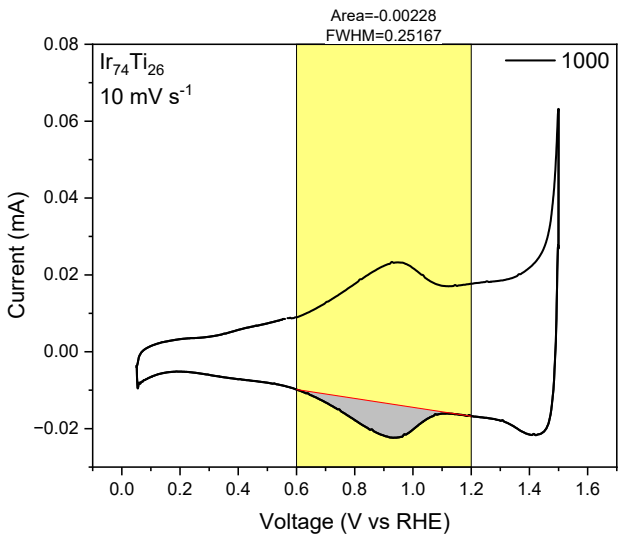

Figure S8. Quantification of electrochemically active sites. Integral of reductive portion of the main redox peak. Cyclic voltammogram measured at 10 mV s^{-1}

If assuming that that all electrochemically active iridium atoms simultaneously undergo a single electron transition during the main redox event around 1.0 V vs RHE, Faraday law can be applied to calculate the charged flowing by simply accounting for the cyclic voltammogram scan rate:

$$Q = \frac{1}{\nu}\int i\,dV$$

Where Q is the charge in mC, v is the scan rate of the cyclic voltammogram, i is the current in mA and V is the voltage in volts.

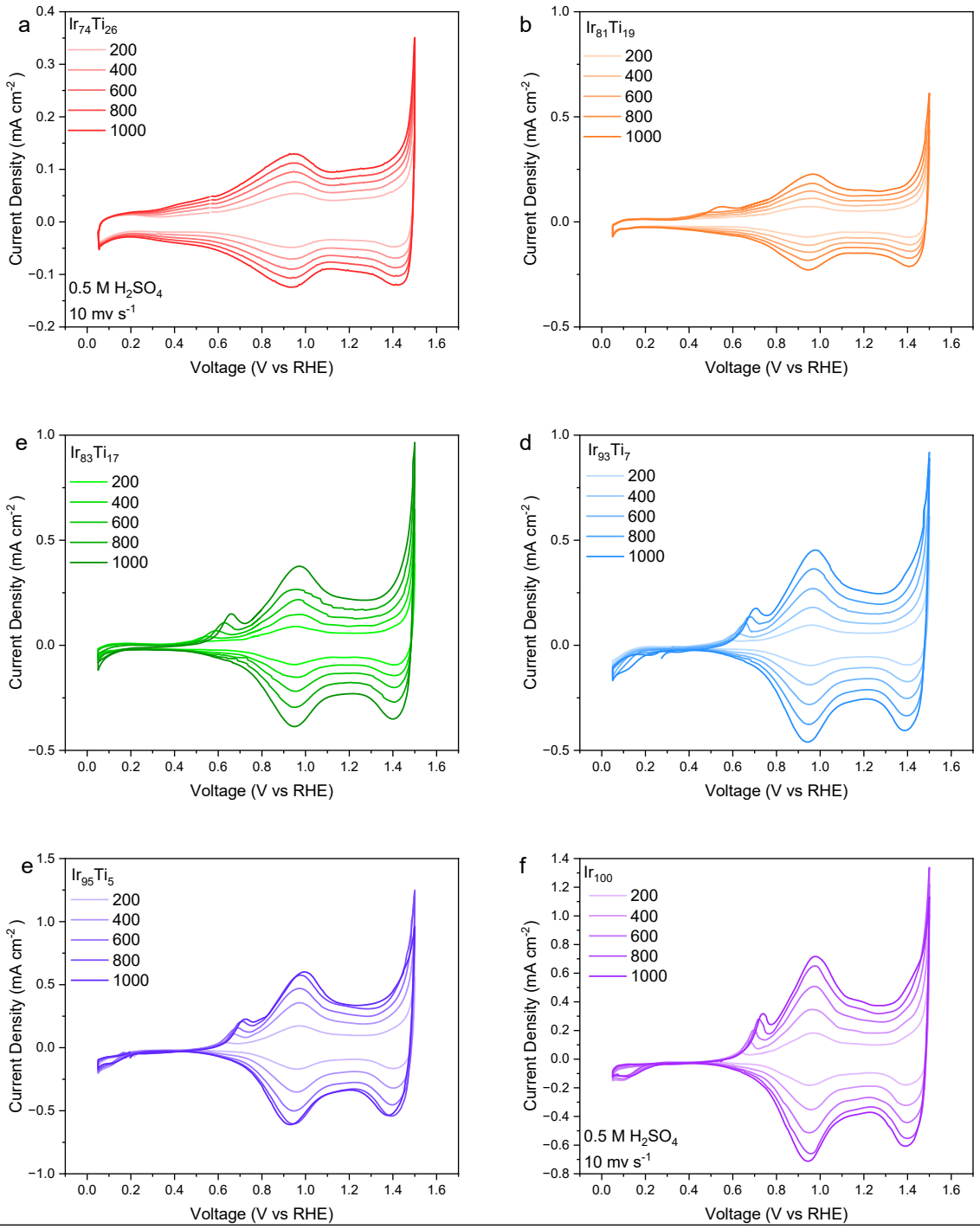

Figure S9. Growth of am-hydr-IrOx via potential cycling between 200-1000 cycles. Samples were cycled at 500 mV s^{-1} for 200 cycles, followed by one measurement at 10 mV s^{-1} which are displayed here.

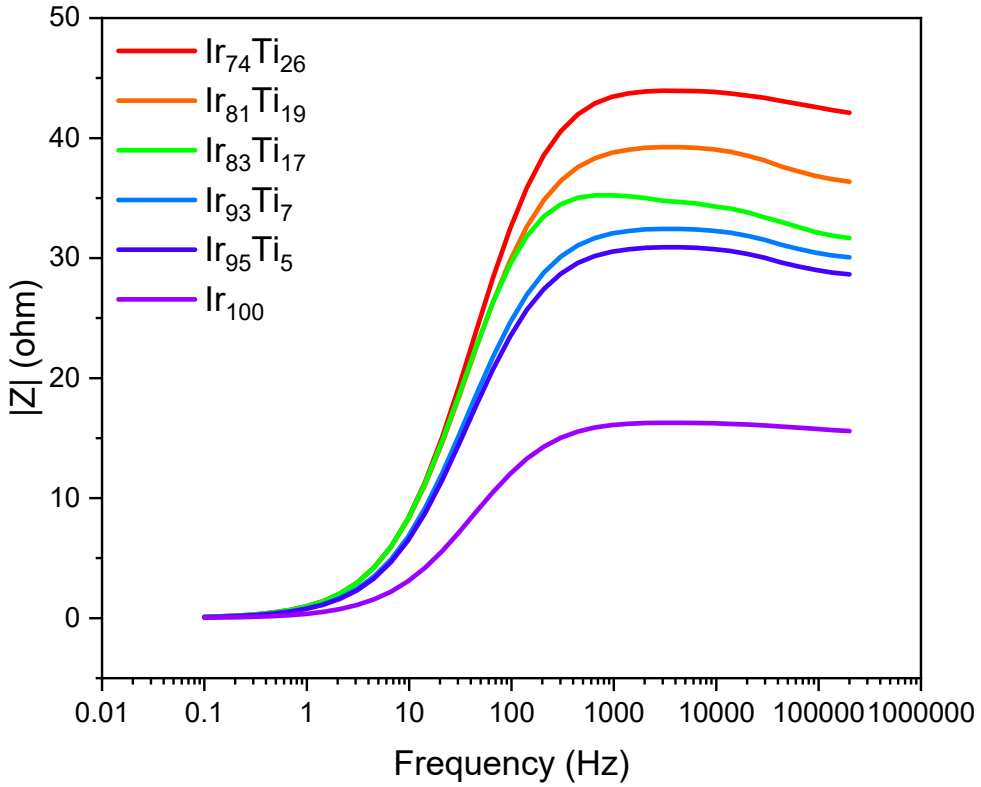

Figure S10. Bode representation of electrochemical impedance spectra of 1000-cycle am-hydr-IrOx layers grown from IrTi alloys with different Ir content.

Hard X-ray photoelectron spectroscopy (HAXPES) measurements

The samples for these experiments were prepared by cycling up to 1000 cycles in the same methodology as for the electrochemical experiments reported here.

No attempts to quantify the thickness of the surface am-hydr-IrO_x were performed, since the measurements were taken under UHV conditions, and loss of water from the structure could result in collapse, or simply density changes can interfere with the calculations giving inaccurate estimations of the layer thickness. Additionally, the Ir 4f was the only measured region at 6 keV due to poorer flux leading to low statistics.

Note: The samples used in this experiment were produced in an identical way, however, due to the non-automated closing of shutters during the sputtering procedure, the surface composition is slightly different (see Table S4). Since electrochemical growth penetrates deep into the bulk of the metallic alloy, these slight differences at the surface composition do not affect the electrochemical behavior significantly. Therefore, the bulk elemental ratio between the two samples batches is likely quite similar.

The different elemental surface ratios are shown in Fig. 3 and summarized below.

Ir power (W)	Ti power (W)	Elemental ratio for sample batch used for Ti K-edge XAS measurements	Elemental ratio for sample batch used in all other experiments
50	80	$Ir_{65}Ti_{35}$	$Ir_{74}Ti_{26}$
50	60	$Ir_{73}Ti_{27}$	$Ir_{81}Ti_{19}$
50	40	$Ir_{81}Ti_{19}$	$Ir_{83}Ti_{17}$
50	20	$Ir_{89}Ti_{11}$	$Ir_{93}Ti_{7}$
50	10	$Ir_{91}Ti_{9}$	$Ir_{95}Ti_{5}$
50	0	Ir_{100}	Ir_{100}

Table S4 Summary of the obtained elemental ratios of the Ir_xTi_{1-x} alloys used for different experiments.

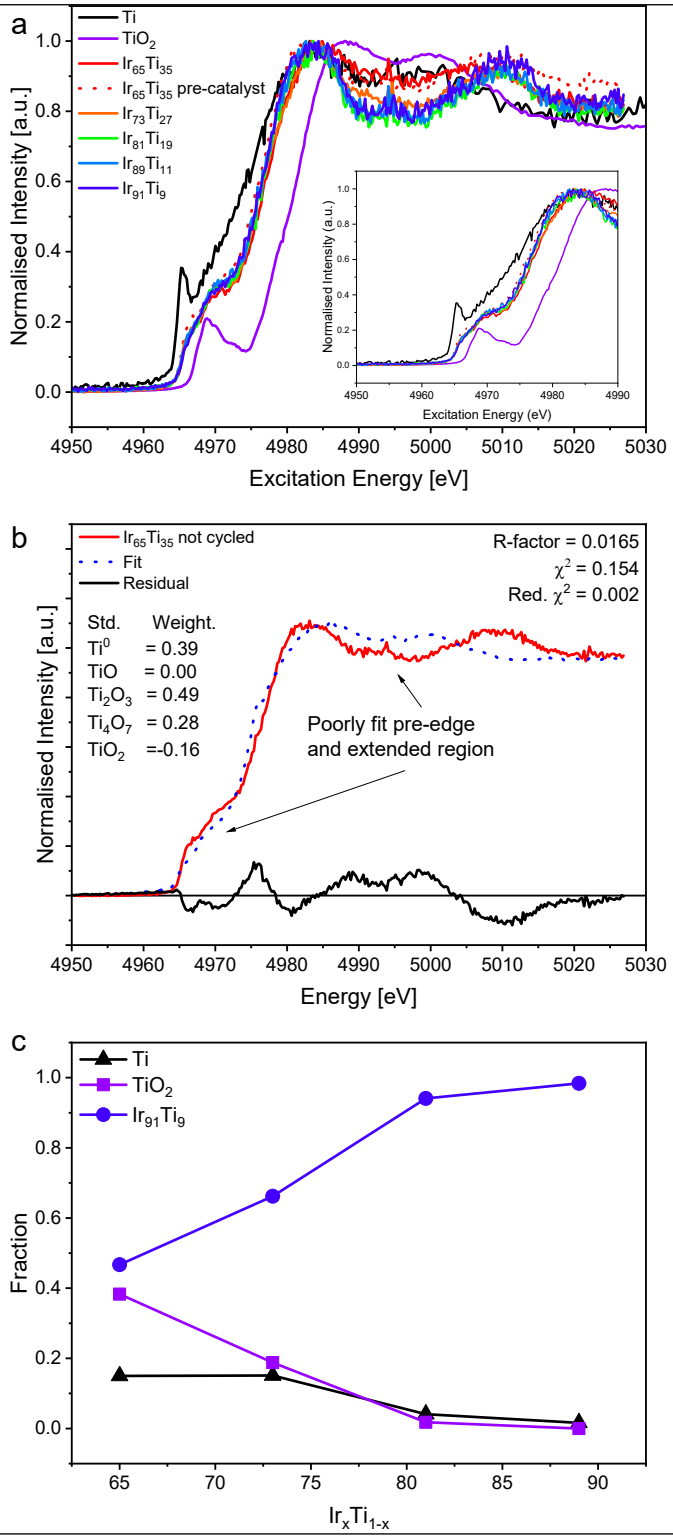

Figure S11 X-ray absorption spectroscopy of Titanium K-edge. (a) Comparison of measured spectra of the 1000-cycle am-hydr-IrO_x/Ir_xTi_{1-x} samples with metallic titanium and (amorphous) titanium oxide references. The inset highlights the differences between the spectra in the pre-edge and white line region of the samples in comparison to the reference spectra. (b) Linear combination fit of the spectrum of the $Ir_{65}Ti_{35}$ film using reference spectra of Ti, TiO, Ti_2O_3, Ti_4O_7, and TiO_2. The arrows highlight spectral regions that are only poorly described by this fit approach. (c) Composition of the studied am-hydr-IrO_x/Ir_xTi_{1-x} samples as derived by a linear combination fit using the spectrum of the sample with the lowest titanium content ($Ir_{91}Ti_9$) together with Ti and (amorphous) TiO_2 reference spectra.

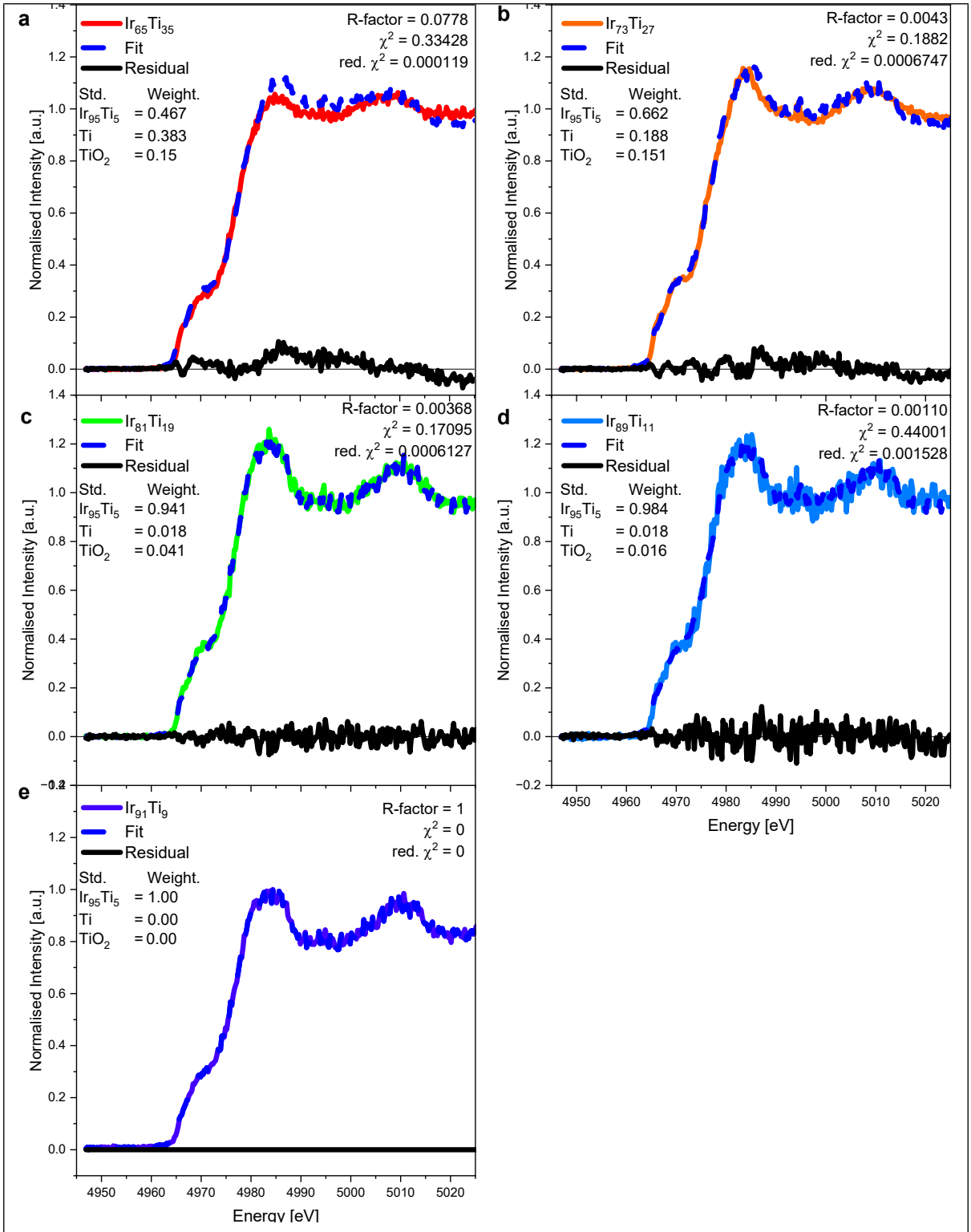

Figure S12 Linear combination fit of the titanium K-edge XAS spectra using $Ir_{91}Ti_9$, Ti, and TiO_2 as fit components. Within each spectrum, the fitting statistics and weights of the standards are given.

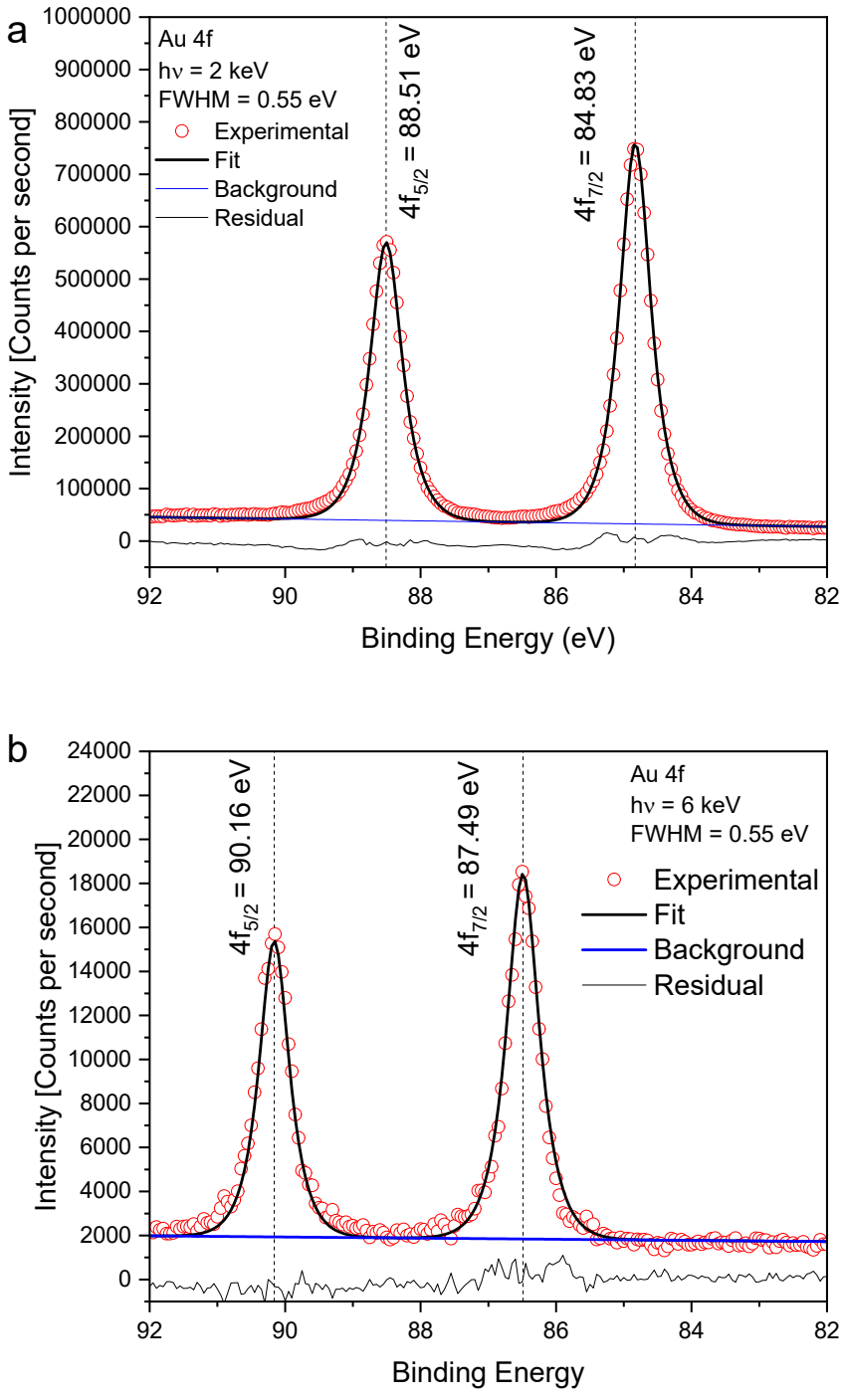

Figure S13 HAXPES detail spectra of Au 4f for calibration. Au 4f data of a clean Au foil recorded with 2 (top) and 6 (bottom) keV excitation energy. Peaks are fit using GL(83) line shape after subtracting a linear background using CasaXPS software. Spectra were recorded using a pass energy of 20 eV. All data was calibrated by shifting the Au $4f_{7/2}$ line to a binding energy of 84.00 eV.

Electrochemical Activity

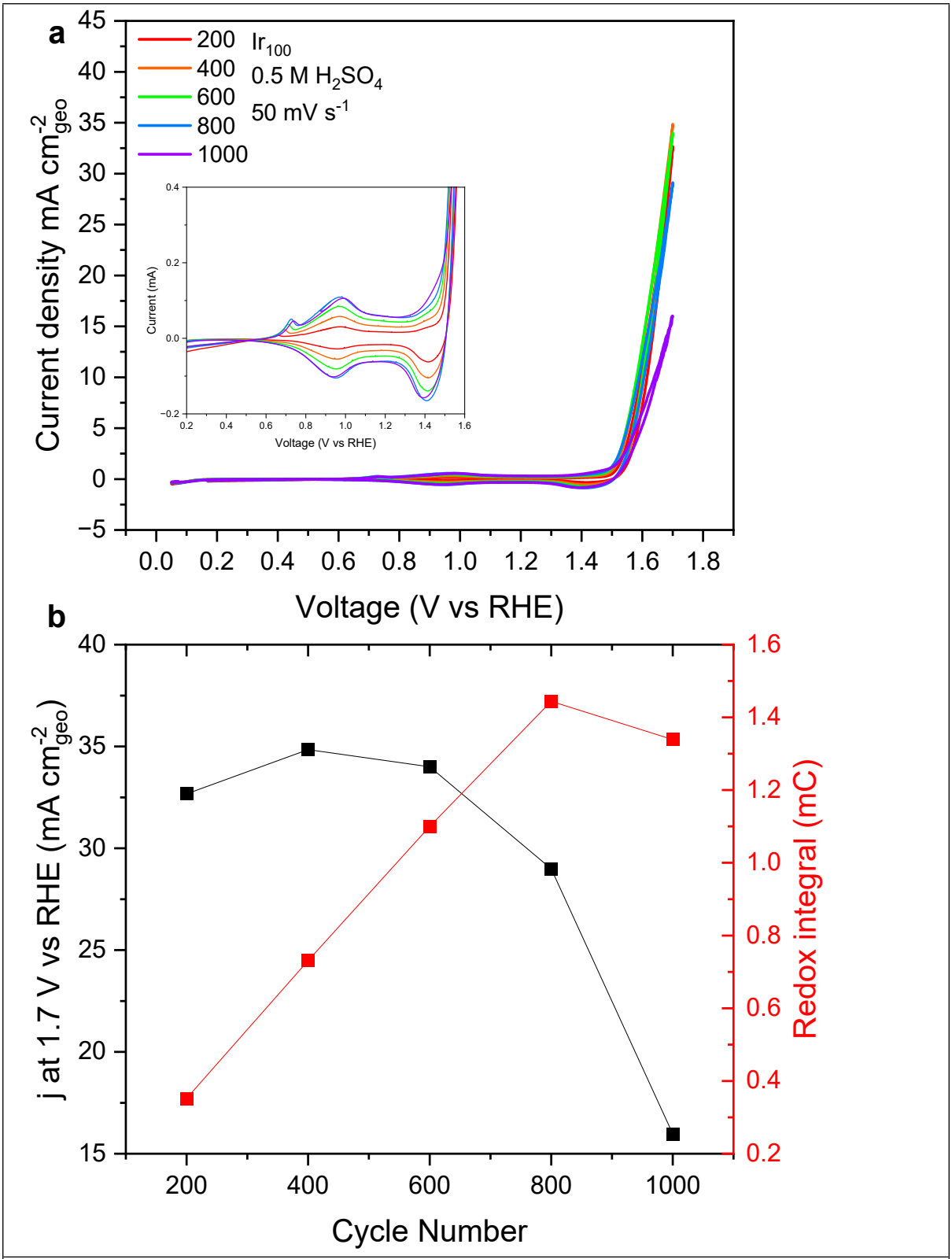

Figure S14 Activity of am-hydr-IrOx grown on Ir_{100} as a function of cycle number. (a) cyclic voltammetry of Ir_{100} between 0.05 to 1.7 V vs RHE. The inset shows pseudocapacitive region, highlighting growth of am-hydr-IrO_x. (b) Current at 1.7 V vs RHE and the redox integral (calculated in same method as shown in **Fig S8**) as a function of cycle number.

***Operando* X-ray absorption spectroscopy at the Ir L_3-edge**

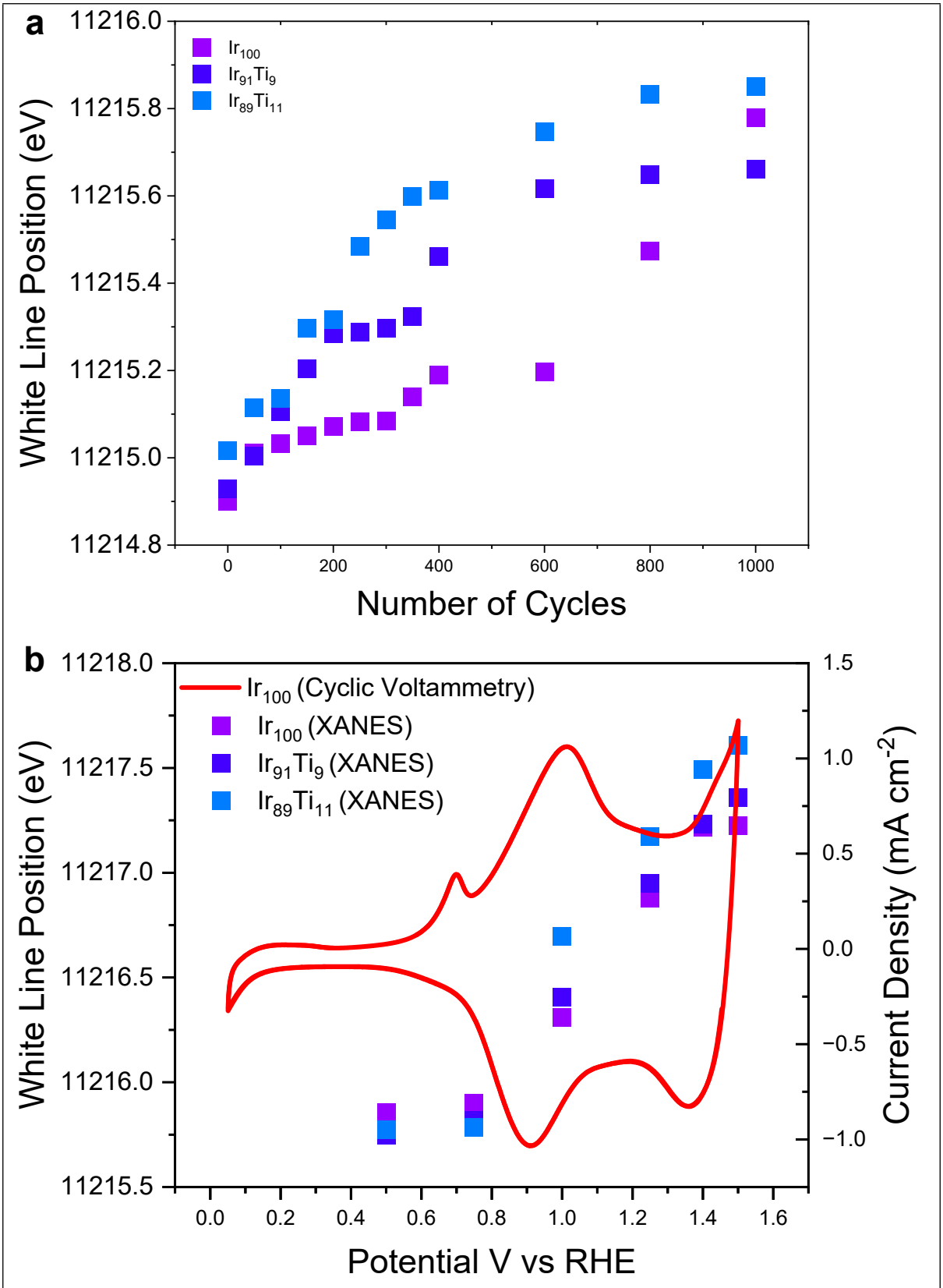

Figure S15 *Operando* X-ray absorption spectroscopy at the Ir L_3-edge. (a) White line position as a function of am-hydr-IrO_x growth cycles using different Ir_xTi_{1-x} films. (b) White line position as a function of potential in direct comparison with the current density as a function of potential.

Electrochemical Stability

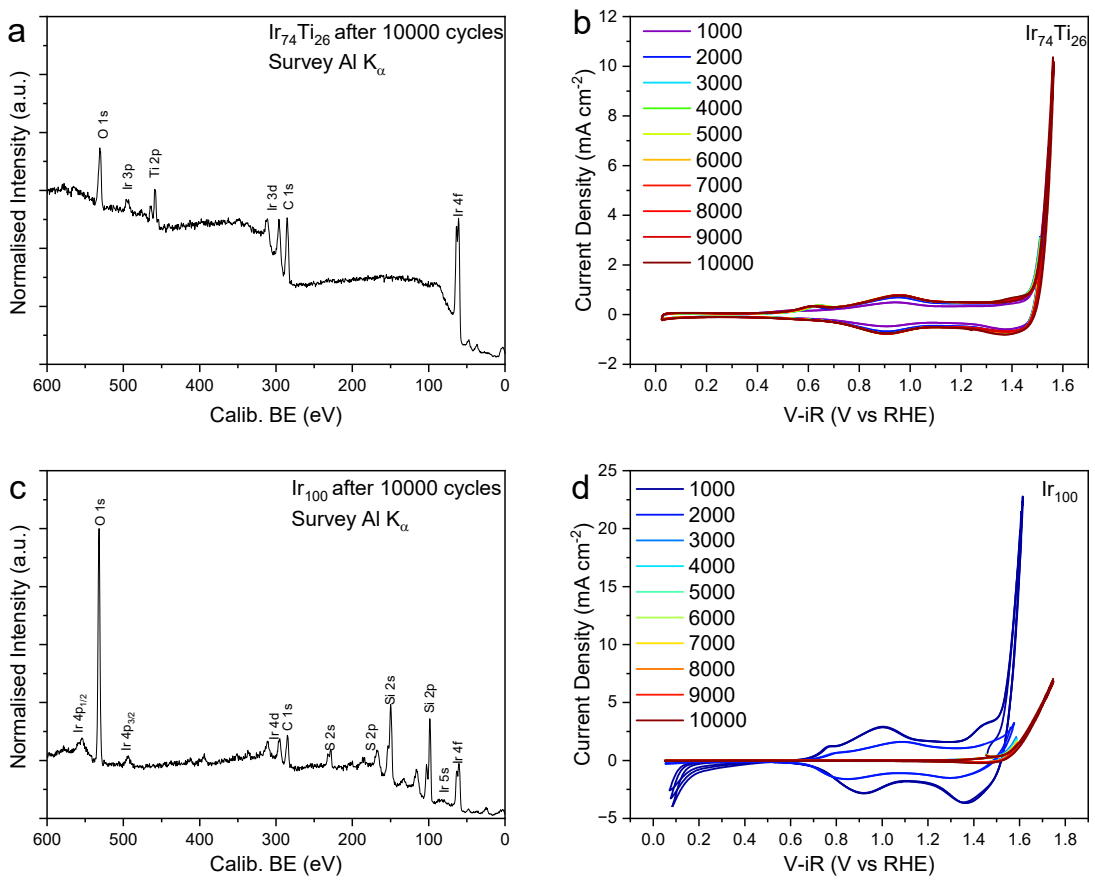

Figure S16 Accelerated degradation tests and post-mortem analysis of am-hydr-IrOx grown on Ir_{100} and $Ir_{74}Ti_{26}$ (a) Al K_α excited XPS survey spectrum of the $Ir_{74}Ti_{26}$ based sample. (b) Cyclic voltammetry of the $Ir_{74}Ti_{26}$ based sample between 1000 and 10000 cycles. (c) Al K_α XPS survey spectrum of the Ir_{100} based sample. (d) Cyclic voltammetry of the Ir_{100} based sample between 1000 and 10000 cycles.

The presence of S in Fig. S16c is interpreted to originate from H_2SO_4 from the electrolyte that was not entirely removed from washing with deionized water.

Ti 2p region for cycled films

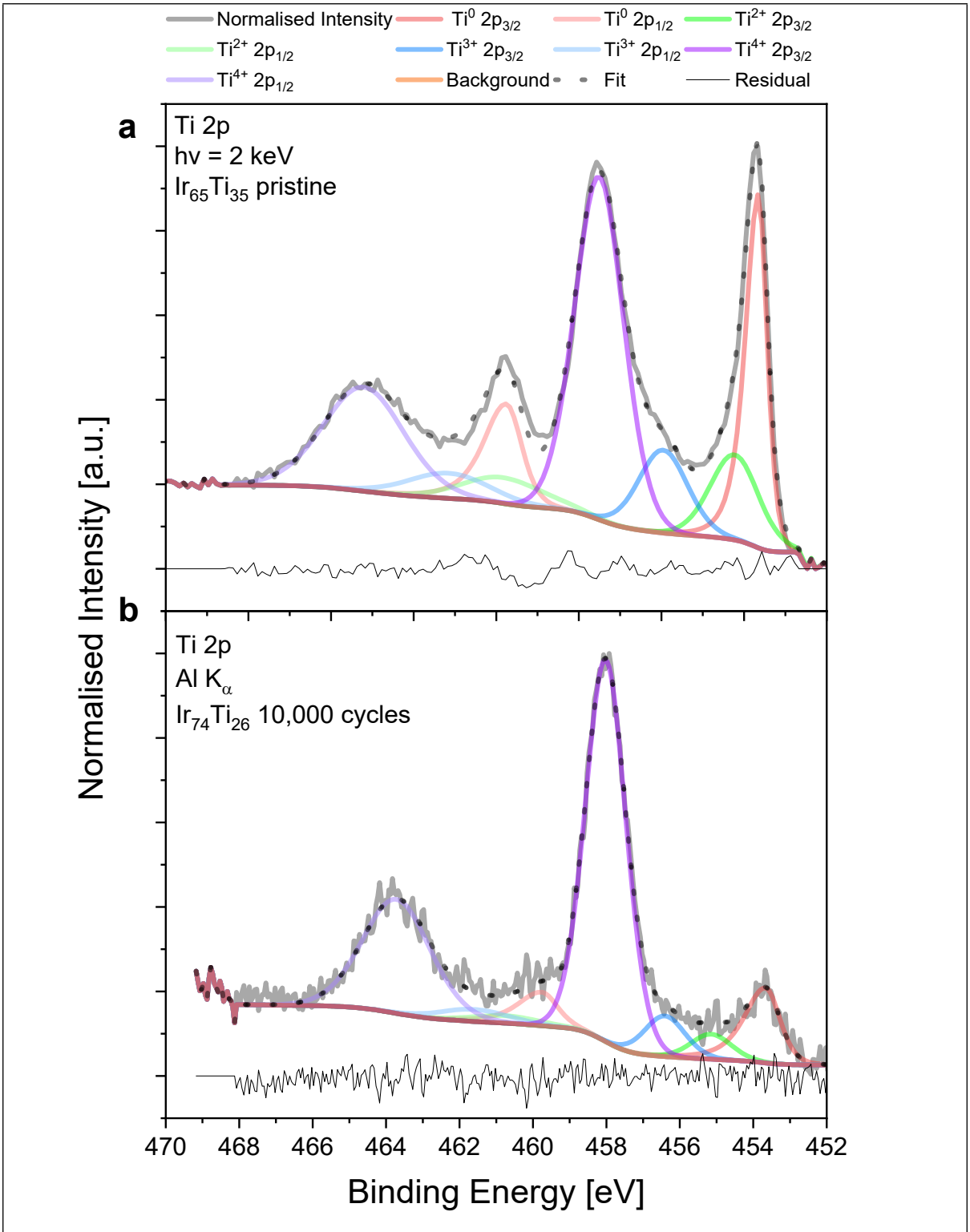

Figure S17 HAXPES/XPS spectra fit of the Ti 2p region of the pristine sample compared to that grown to 10000 cycles. (a) HAXPES spectrum of the pristine $Ir_{65}Ti_{35}$ alloy film measured with 2 keV excitation energy. (b) XPS spectrum of the $Ir_{74}Ti_{26}$ based sample after 10000 cycles electrochemical growth measured with an Al K_α source.

References

1. van der Merwe, M. *et al.* The Chemical and Electronic Properties of Stability-Enhanced, Mixed Ir-TiOx Oxygen Evolution Reaction Catalysts. *ACS Catal.* **13**, 15427–15438 (2023).

2. Trzhaskovskaya, M. B., Nefedov, V.I., Yarzhemsky, V.G., Photoelectron Angular Distribution Parameters for Elements Z = 1 to Z = 54 in the Photoelectron Energy Range 100 – 5000 eV, Atomic Data and Nuclear Data Tables **77,** 97–159 (2001) and Trzhaskovskaya, M. B., Nefedov, V.I., Yarzhemsky, V.G., Photoelectron Angular Distribution Parameters for Elements Z = 55 to Z = 100 in the Photoelectron Energy Range 100 – 5000 eV, Atomic Data and Nuclear Data Tables **82,** 257–311 (2002).

3. Biesinger, M. C., Lau, L. W. M., Gerson, A. R. & Smart, R. St. C. Resolving surface chemical states in XPS analysis of first row transition metals, oxides and hydroxides: Sc, Ti, V, Cu and Zn. *Applied Surface Science* **257**, 887–898 (2010).

4. Gorgoi, M. *et al.* The high kinetic energy photoelectron spectroscopy facility at BESSY progress and first results. *Nuclear Instruments and Methods in Physics Research Section A: Accelerators, Spectrometers, Detectors and Associated Equipment* **601**, 48–53 (2009).

5. Schaefers, F., Mertin, M. & Gorgoi, M. KMC-1: A high resolution and high flux soft x-ray beamline at BESSY. *Review of Scientific Instruments* **78**, 123102 (2007).

6. Devienne, A. & García-Fusté, M. J. Shielding calculations for the design of new beamlines at ALBA synchrotron. *Radiation Physics and Chemistry* **171**, 108759 (2020).

7. Marini, C. *et al.* BL16 NOTOS, an X-ray absorption and diffraction beamline for operando battery studies at ALBA. *Eur. Phys. J. Plus* **140**, 1228 (2025).

8. Schaefers, F., Mertin, M. & Gorgoi, M. KMC-1: a high resolution and high flux soft x-ray beamline at BESSY. *Rev Sci Instrum* **78**, 123102 (2007).

9. Gorgoi, M., Schäfers, F., Svensson, S. & Mårtensson, N. Relative sub-shell photoionization cross-sections of nickel metal determined by hard X-ray high kinetic energy photoemission. *Journal of Electron Spectroscopy and Related Phenomena* **190**, 153–158 (2013).

10. Scofield, J. H. *Theoretical Photoionization Cross Sections from 1 to 1500 keV.* https://www.osti.gov/servlets/purl/4545040 (1973).